

## Effect of Nuclear Alignment on the 14-MeV Total Neutron Cross Section of $^{165}\text{Ho}$

H. MARSHAK AND A. C. B. RICHARDSON  
National Bureau of Standards, Washington, D. C.

AND

T. TAMURA\*  
Oak Ridge National Laboratory, Oak Ridge, Tennessee  
(Received 30 March 1966)

The effect of nuclear alignment on the total cross section of the highly deformed  $^{165}\text{Ho}$  nucleus has been measured using 14-MeV neutrons. The aligned  $^{165}\text{Ho}$  target was obtained by cooling a metal single crystal to 0.33°K. A finely collimated beam of 14-MeV neutrons was produced by careful collimation of the alpha particle produced in the  $^3\text{H}(d,n)^4\text{He}$  reaction and by detecting it in fast coincidence with its associated neutron. The measured total cross section is  $5.29 \pm 0.10$  b. The fractional change in the total cross section, for our value of nuclear alignment ( $f_2=0.31$ ), is  $+(3.52 \pm 0.75)\%$ , where the positive sign indicates a larger cross section for nuclei aligned perpendicular to the incident beam than for randomly oriented nuclei. These results are in excellent agreement with the predictions of the optical model using an adiabatic coupled-channel calculation. The optical-model parameters used are in good agreement with those obtained from other measurements, and in particular the value of the deformation parameter  $\beta = +0.30$  is the same as that used in our earlier work. It was also found that 14 MeV is not yet a sufficiently high energy to use the black-nucleus model to interpret our results.

### I. INTRODUCTION

THE use of oriented nuclear targets to study various properties of nuclei, in particular nuclear deformations, has been discussed in a number of papers.<sup>1-4</sup> The effect of nuclear deformation using an aligned  $^{165}\text{Ho}$  target has been demonstrated in the photoneutron-production cross-section measurements of Ambler *et al.*,<sup>5</sup> and in the neutron cross-section measurements of Wagner *et al.*<sup>6</sup> There have also been some recent neutron measurements made by Shelley *et al.*<sup>7</sup> The role of  $^{165}\text{Ho}$  is unique in these measurements since it is a highly deformed mono-isotopic nucleus which can be easily aligned.

The data of Wagner *et al.* (hereafter referred to as WMTM), which were obtained using 350-keV neutrons, were interpreted in terms of the optical model using a coupled-channel calculation.<sup>8</sup> It was pointed out there that such measurements relating to nuclear shapes could be interpreted more definitely and perhaps more easily at higher neutron energies particularly because the contribution of the compound processes becomes less important. Also the adiabatic approximation<sup>8</sup> can be used in the coupled-channel calculation if the neutron energy is sufficiently high compared to the rotational energy of the nucleus. Since the rotational energy for  $^{165}\text{Ho}$  is about 100 keV, one should expect this approximation to be valid at neutron energies of a few MeV or higher. If the neutron energy is further increased (above some tens of MeV), one might perhaps be able to use the black-nucleus model to interpret the results,<sup>2</sup> and the interpretation then is quite straightforward. The exact energy at which the black-nucleus model begins to be valid is, however, uncertain. At still higher energies the situation will become complicated once again since the nucleus is expected to become semitransparent to the neutron. For the interpretation of such high-energy data the theory of Inopin<sup>9</sup> may well be used.

Since a highly monoenergetic beam of 14-MeV neutrons can be obtained using the  $^3\text{H}(d,n)^4\text{He}$  reaction, and optical-model parameters are available for comparison in this energy region, both for holmium<sup>10</sup> and other nuclei,<sup>11</sup> measurements were undertaken of the effect of nuclear deformation on the total cross section using an aligned  $^{165}\text{Ho}$  target. At 14 MeV the adiabatic

\* Research sponsored by the U. S. Atomic Energy Commission under contract with the Union Carbide Corporation.

<sup>1</sup> A. M. Baldin, in *Proceedings of the All Union Conference on Low and Medium Energy Nuclear Reactions* (Academy of Sciences Moscow, 1957), p. 479; Nucl. Phys. **9**, 237 (1958).

<sup>2</sup> G. L. Visotskii, E. V. Inopin, and A. A. Kresnin, Zh. Eksperim. i Teor. Fiz. **36**, 574 (1959) [English transl.: Soviet Phys.—JETP **9**, 398 (1959)]; see also S. Z. Drozdov, Zh. Eksperim. i Teor. Fiz. **28**, 734 (1955) [English transl.: Soviet Phys.—JETP **1**, 588 (1955)].

<sup>3</sup> E. G. Fuller and E. Hayward, in *Nuclear Reactions*, edited by P. M. Endt and P. B. Smith (North-Holland Publishing Company, Amsterdam, 1962), Vol. II, p. 113.

<sup>4</sup> K. T. R. Davies, G. R. Satchler, R. M. Drisko, and R. H. Bassel, Nucl. Phys. **44**, 607 (1963).

<sup>5</sup> E. Ambler, E. G. Fuller, and H. Marshak, Phys. Rev. **138**, B117 (1965).

<sup>6</sup> R. Wagner, P. D. Miller, T. Tamura, and H. Marshak, Phys. Rev. **139**, B29 (1965); hereafter referred to as WMTM. In this work the total-neutron cross section was measured using a beam of 350-keV polarized neutrons and a polarized target. The effect of nuclear deformation depends only upon nuclear alignment, and the use of a polarized beam and a polarized target can lead to erroneous results unless one first demonstrates that spin-spin effects in the interaction are negligible, as was done by WMTM.

<sup>7</sup> E. G. Shelley, T. R. Fisher, R. S. Sofrata, J. McCarthy, and S. M. Austin, Phys. Letters **19**, 684 (1966). These measurements were made at neutron energies of 8 and 15 MeV and using a polarized target.

<sup>8</sup> T. Tamura, Rev. Mod. Phys. **37**, 679 (1965).

<sup>9</sup> E. V. Inopin, Zh. Eksperim. i Teor. Fiz. **30**, 210 (1956) [English transl.: Soviet Phys.—JETP **3**, 134 (1956)].

<sup>10</sup> T. Tamura, Phys. Letters **9**, 334 (1964); **12**, 121 (1964).

<sup>11</sup> F. G. Perey and B. Buck, Nucl. Phys. **32**, 353 (1962).

coupled-channel calculation is certainly expected to apply in the interpretation of our experimental results, and as we shall see in Sec. V, this is in fact the case. On the other hand it is also seen there that this energy is too low to use the black-nucleus model.

Since the effects of nuclear deformation on the total cross section only depend upon *nuclear alignment* and *not nuclear polarization*, a single crystal<sup>12</sup> of holmium metal cooled to 0.33°K in the absence of a magnetic field was used as our target. This crystal, although rather large (16.505g) for a rare-earth metal crystal, was nonetheless small, in both area ( $\sim 1 \text{ cm}^2$ ) and thickness (1.08 cm), when considered as a nuclear target for 14-MeV neutrons. When one also considers the rather complicated description needed to completely define the nuclear spin system at low temperatures for the crystal in zero-magnetic field (see Sec. III), it would seem better to use a large polycrystalline sample in a high magnetic field. It has also been demonstrated<sup>13</sup> that by increasing the sample thickness (depending upon the available beam intensity and background conditions), the measured effects in the total cross section due to nuclear orientation (either polarization or alignment) are enhanced. Thus, it would seem that a larger and thicker polycrystalline sample in a high magnetic field might be a better choice.<sup>7</sup> In this case we would, of course, have a *polarized* target as well as an *aligned* target. The disadvantage of using such a thick polarized target is that if there is any spin-spin coupling present in the interaction,<sup>6</sup> the unpolarized neutron beam will become polarized as it passes through the sample<sup>14</sup> and second-order effects might lead to slightly erroneous results. Therefore the small, thin single crystal was chosen so that we would *only have an aligned target*.

The small available area of the <sup>165</sup>Ho single crystal and its thickness put stringent requirements on the source of 14-MeV neutrons used, namely, a well-collimated small beam with inherent high counting stability. The last requirement was needed because the change in transmission due to nuclear alignment was expected to be rather small. It was found that by careful use of the associated-particle technique (usually employed for neutron time-of-flight measurements) we were able to obtain the finely collimated 14-MeV neutron beam essential for our target. This method of collimation also has built into it accurate normalization of the neutron intensity, so that the usual neutron monitors (long counters or biased detectors), with their inherent background uncertainties, did not have to be used. The details of this neutron source are explained in Sec. IIA.

In order to check that the effect we observe using our single crystal is really due to nuclear alignment and not

to some systematic error,<sup>15</sup> we also made a series of transmission measurements on a polycrystalline holmium sample (which was similar in shape and size to our single-crystal sample) under identical conditions to the single-crystal measurements. There can, of course, be no net nuclear alignment at any temperature in a polycrystalline sample. This, as well as other details concerning the cryogenic target, is discussed in Sec. IIB.

In Sec. III the alignment of <sup>165</sup>Ho in the form of a holmium-metal single crystal is discussed, and our experimental results are given in Sec. IV. In Sec. VA we present the analysis of our data in terms of the adiabatic coupled-channel calculation, and in Sec. VB a discussion of the predictions of the black-nucleus model is given.<sup>16</sup> Conclusions are presented in Sec. VI, together with remarks about future investigations.

## II. EXPERIMENTAL METHOD

### A. 14-MeV Neutron Source

The expected small effect of nuclear alignment on the total neutron cross section for <sup>165</sup>Ho, along with the relatively thin single-crystal sample available, required a high degree of neutron counting stability; that is, changes in transmission as small as 0.1% had to be measurable. In view of the small area of the <sup>165</sup>Ho sample, the intensity of the available 14-MeV neutron source, and the counting statistics needed for the above accuracy, a small target-to-sample separation was also required. This precluded use of the massive physical collimation normally used for 14-MeV neutrons. Finally, the complicated structure of the <sup>3</sup>He refrigerator around the sample required finding a convenient means for determining the background.

All of these problems were solved by detecting the alpha particle produced in the <sup>3</sup>H(*d,n*)<sup>4</sup>He reaction in coincidence with its associated neutron.<sup>17</sup> Suitable collimation of the alpha particles yielded a small well-defined cone of associated neutrons, so that physical collimation was not necessary. In addition, the coincident alpha pulses provided the accurate and stable neutron normalization required. The alpha pulse was also used to make possible measurement of the neutron time-of-flight for convenient determination of the background.

The NBS 2-MeV Van de Graaff was used to provide a 1- $\mu$ A, 300-keV deuteron beam. Thin Ti-T targets (175  $\mu\text{g}/\text{cm}^2$ ) were used as the neutron source. A

<sup>15</sup> For example, if holmium metal had an abnormally large volume expansion coefficient in the 4.2 to 0.33°K temperature region we would observe an apparent change in the cross section when in reality the nuclear density was changing.

<sup>16</sup> A short report of this work has been published: H. Marshak, A. C. B. Richardson, and T. Tamura, Phys. Rev. Letters **16**, 194 (1966). The measured values for  $\sigma_t$  and  $\Delta\sigma_t$  quoted in the present paper are slightly different from those reported previously because of improved handling of the in-scattering correction.

<sup>17</sup> See, e.g., G. K. O'Neill, Phys. Rev. **92**, 853 (1953); and J. Rethmeier *et al.*, Nucl. Instr. Methods **17**, 273 (1962).

<sup>12</sup> The authors are grateful to Dr. S. Legvold and Dr. F. H. Spedding for lending us this crystal.

<sup>13</sup> H. Marshak, Bull. Am. Phys. Soc. **7**, 305 (1962). It was shown in this work that even for very small nuclear polarization (<1%) measurable effects can still be obtained using almost black samples.

<sup>14</sup> M. E. Rose, Nucleonics **3**, 23 (1948).

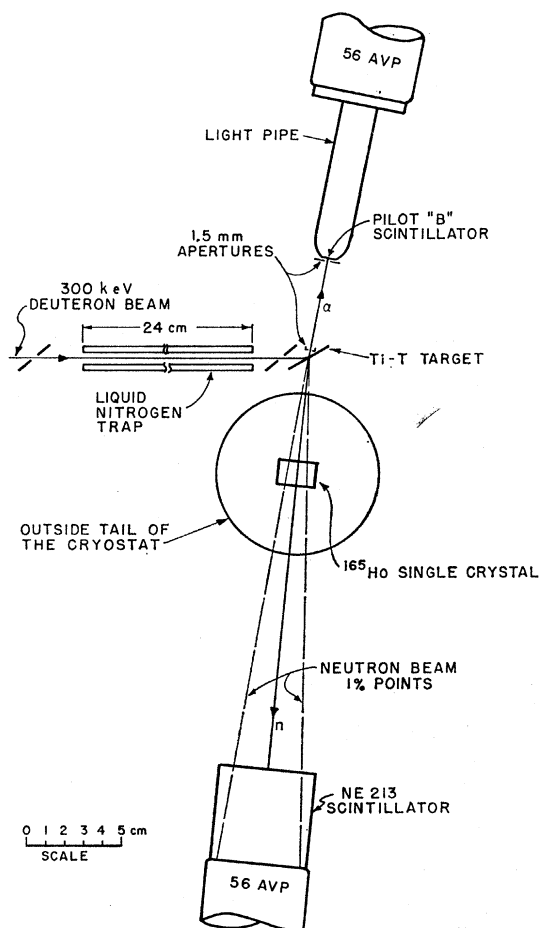


Fig. 1. The experimental arrangement.

schematic diagram of the apparatus is shown in Fig. 1. The alpha detector was placed at an angle of  $78.5^\circ$ ; the correlated 14-MeV neutrons are then located at approximately  $90^\circ$ . The deuteron beam was collimated by a double elliptical aperture of just such dimensions as to provide a circular target area when viewed along the axis of the alpha collimator. The diameter of this area was chosen to be 50% larger than the effective diameter of the alpha collimator. This provided an adequate safety margin against any misalignment or flexing of the target backing, but at the same time still minimized the production of background neutrons from target area not seen by the alpha detector. Since small-angle scattering of either an incident deuteron or product alpha particle affects the direction of the associated neutron, the target surface must be kept free of contaminants from the accelerator vacuum system. A cold trap close to the target surface, cooled by liquid nitrogen, reduced the rate of this buildup to a few percent of the rate without a trap. The target was mounted in an eccentric holder so that it could be rotated to a new position after several days of running. By this means all of the runs within any one of the three series of measurements

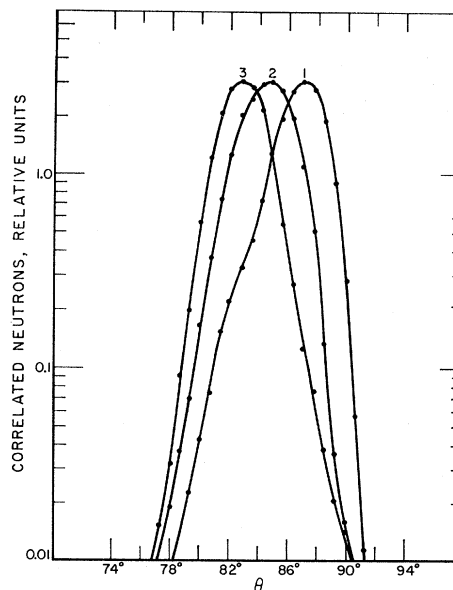


Fig. 2. Correlated neutron-beam profiles taken in the reaction plane. These three profiles were taken at different times during the lifetime of the Ti-T target. The first one (1) is for a fresh target, (2) after approximately 60 h of use ( $\sim 200$  mC of deuteron bombardment), and (3) after approximately 100 h of use ( $\sim 350$  mC of deuteron bombardment).

(polycrystalline  $^{165}\text{Ho}$  in air, single-crystal and then polycrystalline  $^{165}\text{Ho}$  in the cryostat) were made using the same target.

Although the attainment of a finely collimated neutron beam might at first thought seem only to involve reduction of the alpha collimator aperture, Coulomb scattering effects soon become important. The associated neutron spatial distribution was investigated as a function of target thickness and age, as well as of alpha collimator size.<sup>18</sup> It was found that significant contributions to the observed beam widths are made by Coulomb scattering of the deuteron and alpha particles

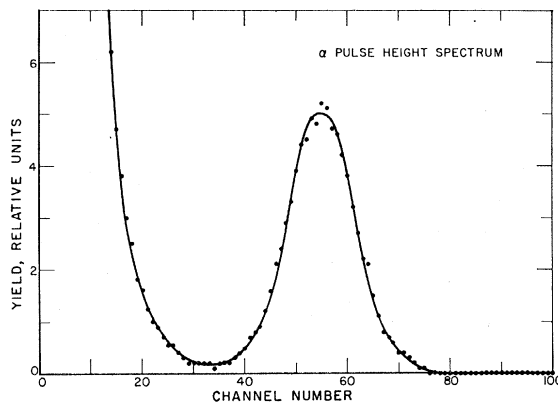


Fig. 3. The  $\alpha$  pulse-height spectrum. The discriminator was set at channel 34.

<sup>18</sup> A more detailed account will be found in A. C. B. Richardson, H. Marshak, R. B. Schwartz, and E. Ritter (to be published).

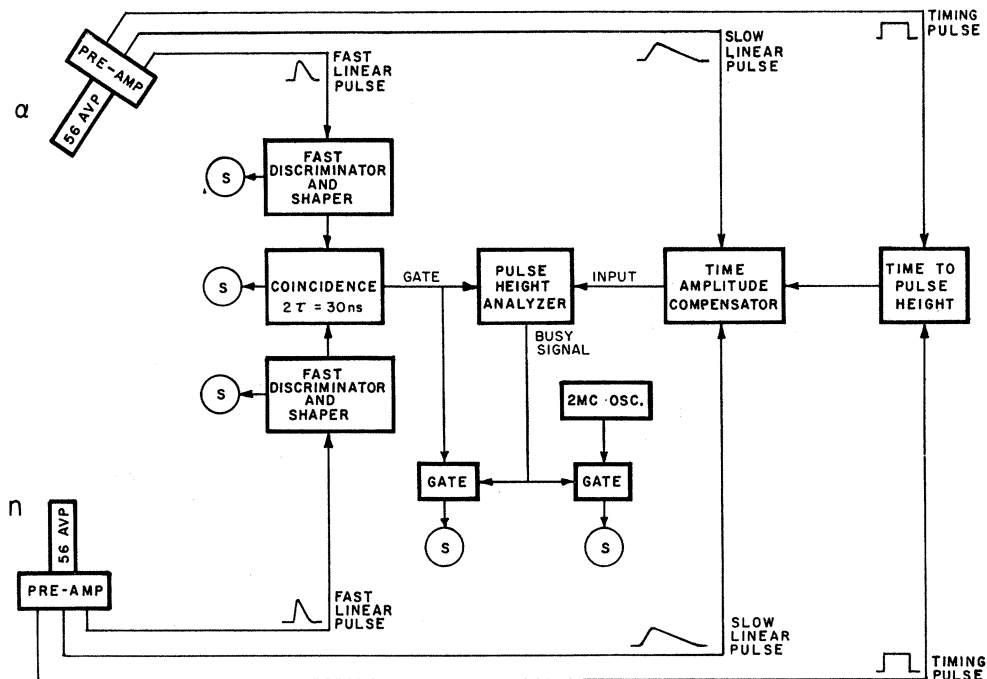


Fig. 4. Block diagram of the electronics. Scalers are indicated by the letter S.

in the target. In addition, the neutron beam moves backwards as the target ages. This is due to an increase in the average deuteron energy loss resulting from buildup of surface contamination and loss of tritium from the target surface. The above effects are illustrated by the horizontal beam profiles shown in Fig. 2. These profiles were measured by locating the neutron detector 160 cm from the target and then moving it in the reaction plane along the perpendicular to the correlated neutron beam direction. Vertical beam profiles were made in a similar way by moving the detector along the perpendicular to the reaction plane at the maximum of the horizontal profile. We observed a larger beam width in the reaction plane than perpendicular to it; this is caused by reaction kinematics. It was also found that the vertical beam profile does not change significantly as the target ages. Titanium targets, rather than the more common zirconium targets, were used because of the  $Z^2/A$  dependence of Coulomb scattering. Using targets approximately  $175 \mu\text{g}/\text{cm}^2$  thick we found it possible to obtain both a reasonable counting rate and a usable beam size. The beam size at the position of the holmium sample, with the cryostat located as closely as possible to the target housing, was 10.1 mm in the horizontal plane and 7.0 mm in the vertical plane (1% intensity points). With the cryostat in this position the center of the holmium sample was 6.2 cm from the target. It was necessary to move the cryostat periodically as the target aged in order to keep the neutron beam centered on the sample. The procedure used for this alignment is described in Sec. IIB. The neutron energy was  $14.0 \pm 0.1$  MeV. This spread in energy is small in spite of the

effects discussed above, because of the well-known insensitivity of neutron energy near  $90^\circ$  to incident deuteron energy and angle for this reaction.<sup>19</sup>

The alpha detector must distinguish the 3.7-MeV  ${}^3\text{H}(d,n){}^4\text{He}$  alpha from deuteron, helium-3, proton, and triton contributions from the accompanying  ${}^2\text{H}(d,d){}^2\text{H}$ ,  ${}^2\text{H}(d,n){}^3\text{He}$ , and  ${}^2\text{H}(d,p){}^3\text{H}$  interactions. A  $1.6 \text{ mg}/\text{cm}^2$  thick Pilot-B plastic scintillator with an  $0.8 \text{ mg}/\text{cm}^2$  thick aluminum layer evaporated on its face was used to accomplish this discrimination. The aluminum is sufficiently thick to absorb the scattered deuterons, as well as most of the energy of the helium-3. The scintillator thickness was chosen to be just the residual range of the alpha after traversing the aluminum layer, so that the proton passes right through the scintillator with only a small energy loss. The triton is more troublesome; its light output in the scintillator is about 30% that of the alpha. It was excluded by an appropriate setting of the alpha pulse-height discrimination level. The scintillator was located 5.5 cm from the target and coupled to its 56 AVP photomultiplier by an 8.9-cm long light pipe shaped so as to provide total internal reflection for light originating in the scintillator. A typical alpha pulse-height spectrum is shown in Fig. 3. Tests with a driven-in deuterium target showed successful discrimination between the alpha particle and products of competing reactions. The neutron detector was a  $5.1 \text{ cm} \times 5.1 \text{ cm}$  aluminum-walled cylindrical NE 213 liquid-scintillator cell mounted directly to the face of a 56 AVP photomultiplier. The discrimination

<sup>19</sup> J. Benveniste and J. Zenger, University of California Radiation Laboratory Report No. UCRL-4266, 1954 (unpublished).

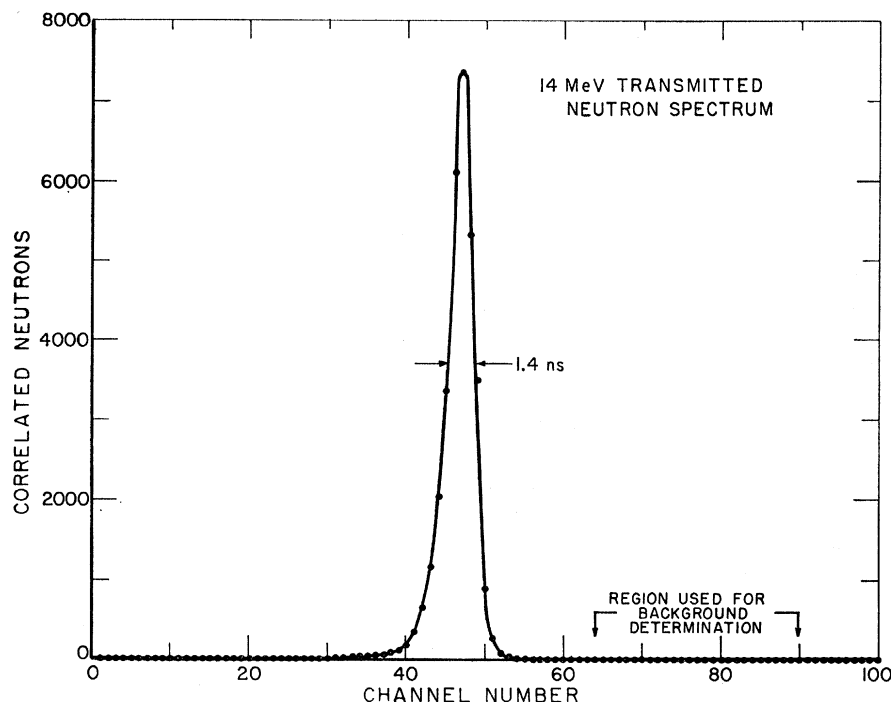


FIG. 5. Correlated neutron time-of-flight spectrum with the cryogenic target in place.

level was set at a proton recoil energy of about 1 MeV. During the transmission measurements the center of the neutron detector was located 25.6 cm from the target. At this distance the beam was 4.2 cm wide and 2.9 cm high.

The electronic circuitry is basically a "fast-slow" system, as shown in Fig. 4, with the alpha and neutron channels identical. The fast signal (timing) is produced by using the photomultiplier anode signals to drive 7788 pentode limiters to cutoff; these outputs are then clipped to a length of 30 nsec by a shorted line. The time converter<sup>20</sup> measures the overlap of the two timing pulses and does not distinguish the sequence in which they arrive. The converter output is fed to an adding circuit, where slow linear dynode signals are used to correct slight timing shifts due to signal amplitude variations, and then into a multichannel pulse-height analyzer. The "slow" legs (amplitude discrimination and negative time elimination) use fast linear dynode pulses to drive fast discriminators.<sup>21</sup> The discriminator outputs are shaped and placed in coincidence ( $2\tau=30$  nsec) to drive the pulse-height analyzer gate. The delay between the two channels was chosen to eliminate the unwanted half of the double-valued time converter output. This has the effect of reducing the accidental background by a factor of 2. The over-all system timing resolution was 1.4 nsec (full width at half-maximum, FWHM) for 14-MeV neutrons, using a 1-MeV proton-recoil discrimination level (see Fig. 5).

<sup>20</sup> The circuit is a modification of an earlier design [J. H. Green and J. Bell, *Nucl. Instr. Methods* **3**, 127 (1958)] by E. R. Mosburg (private communication); see also Ref. 18.

<sup>21</sup> H. Verweij, *Nucl. Instr. Methods* **10**, 308 (1961).

The pulse-height analyzer "busy signal" is employed both to gate the output of a 2-Mc/sec oscillator to a fast scaler and to gate the coincidence output to an additional scaler. This provided two methods for determining losses due to pulse-height analyzer dead time. These measured losses were of the order of one percent by both methods. The time constants of all circuitry preceding the pulse-height analyzer are sufficiently short to contribute negligible additional dead time. A punched paper-tape readout of the pulse-height analyzer was employed to facilitate computer handling of background subtraction.

### B. Aligned <sup>165</sup>Ho Target

The oriented holmium nuclear target used in this experiment was the same as that used in WMTM; that is, the NBS <sup>3</sup>He refrigerator was used to cool a single crystal of holmium metal to 0.33°K. The cryogenic details of the <sup>3</sup>He refrigerator have been discussed in previous papers.<sup>22,5</sup> Since the present measurements depend upon nuclear alignment and not nuclear polarization, a magnetic field is not necessary. For this reason the superconducting split solenoid (see Fig. 6) was not used and the soft-iron magnetic shield surrounding the room-temperature tail of the cryostat was removed. The temperature of the crystal was determined by vapor-pressure readings of the <sup>3</sup>He and checked by calibrated resistance thermometers. During the course of a typical nine-hour measurement (see Sec. IVB) the temperature was 0.33°K, with a stability of 0.01°K.

<sup>22</sup> E. Ambler, R. B. Dove, and R. S. Kaeser, *Advances in Cryogenic Engineering* (Plenum Press, Inc., New York, 1963), p. 443.

The technique for physically aligning the holmium crystal inside the cryostat with respect to the neutron beam was different from that used in WMTM. The alignment had to be improved by a factor of 3 for these measurements; that is, reproducible beam positions to  $\pm 0.5$  mm were required. This was needed for two reasons; first the effect due to nuclear alignment would probably be smaller at 14 MeV than at 350 keV, and second, our present beam size is larger than that used before. In fact, in the horizontal plane the 1% points of the beam profile are about at the limits of the flat part of the crystal (see Fig. 7). However, most of the beam is concentrated within a smaller area (at the 5% points the beam measured 7.3 mm $\times$ 4.5 mm), and the crystal thickness outside the flat portion of the crystal decreases only gradually. A calculation shows that for a 0.5 mm shift in beam position the transmission changes by much less than the 0.1% transmission reproducibility desired. The alignment problem is further complicated since we do not have a physical collimator and the beam moves toward back angles as the Ti-T target ages, as described in the previous section. We describe the aligning procedure used.

In Fig. 6, the lower tails of the cryostat are shown with the alignment jig in place. This jig consists of an aluminum cylinder which fits over the room-temperature tail of the cryostat and has two windows 180° apart on its sides into which cross hairs, telescoping pointers, or a light source may be fastened. With the cross hairs (0.25-mm tungsten wires) on the two windows the cylinder was positioned, by radiography, so that the centerline between these cross hairs (which is also the center of the windows) fell on the center of the holmium crystal and along its *c* axis. The crystallographic axes were determined by x-ray diffraction techniques to an accuracy of  $\pm 1^\circ$ .<sup>23</sup> The accuracy of the alignment of the *c* axis of the crystal relative to the cross hairs of the jig is estimated to be  $\pm 3^\circ$ . Radiographs were made of the crystal cross-hair alignment at 300, 77, 4.2, and 0.33°K. The 4.2 and 0.33°K alignment radiographs are identical, as one would expect; that is, all the shrinkage of the inner tubes of the cryostat (and therefore change in position of the crystal) takes place between 300 and 4.2°K. The jig position was marked to permit its removal and replacement without need for further radiographs.

The following procedure was employed to align the cryostat to the neutron beam before each of the transmission measurements. A horizontal beam profile was measured with the crystal raised out of the beam and the

<sup>23</sup> X-ray diffraction patterns were made at various places on both faces of the crystal. In addition, the crystal had been etched at both tips (top and bottom, see Fig. 7) with nitric acid, revealing plate-like structures. These plates were of the (10 $\bar{1}$ 0) type. X-ray diffraction patterns were also made at both of these tips. All of the x-ray diffraction patterns indicated a single crystal and no evidence for twinning was observed. The x-ray diffraction analysis was kindly done by Dr. C. J. Newton of the National Bureau of Standards.

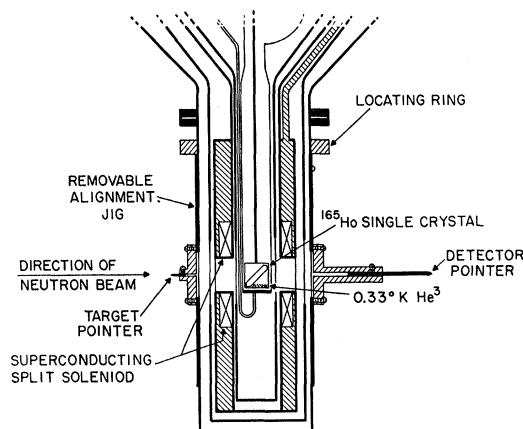


FIG. 6. Schematic drawing of the lower part of the  $^3\text{He}$  cryostat. The removable aligning jig is shown in place.

detector was left at the center of this beam profile. A small telescoping pointer was then fastened to the window of the jig facing the Ti-T target. This target was marked on its back to indicate the intersection of the deuteron beam axis and the axis of the alpha collimator. A light source, capable of focusing a 1.5-mm axial spot of light on the face of the detector, was attached to the other window of the cylinder. The cryostat was positioned so that the pointer coincided with the mark on the target and the light spot with the center of the detector, and securely fastened in place using cables so that no further movement was possible. The light source was finally replaced by a telescoping pointer and the detector moved in and centered at its normal distance for transmission measurements. Fortunately, neutron-beam movement toward back angles was slow enough so that we were able to make at least one 9-h measurement before having to repeat this alignment procedure, which itself takes 3 h:2 h for a beam profile and 1 h for aligning the cryostat. The aluminum jig was always removed before a transmission measurement was started.

Although the sample was accurately aligned for measurements at 4.2°K (no nuclear alignment) and at 0.33°K (partial nuclear alignment), there could possibly be other changes in the experimental apparatus which

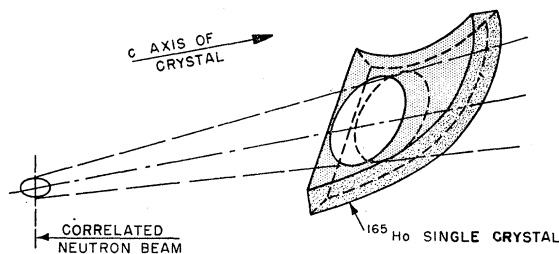


FIG. 7. Location of the holmium single metal crystal with respect to the correlated neutron beam. The *c* axis of the crystal lies along the beam direction.

would lead to erroneous results. If, for example, there were any  $^3\text{He}$  liquid in the way of the beam at  $0.33^\circ\text{K}$  it would result in an increase in the measured holmium cross section. There is, of course, no  $^3\text{He}$  liquid present for the  $4.2^\circ\text{K}$  measurements. Calculations were made assuming the most pessimistic case; that is, all the  $^3\text{He}$  gas (closed system with 1.8 liter of  $^3\text{He}$  at NTP) in the form of liquid at  $0.33^\circ\text{K}$  and in the sample tube. In this case the  $^3\text{He}$  liquid level with the sample in place would be 1.2 mm below the beam. Although this was considered an adequate safety factor, in view of the accuracy of alignment ( $\pm 0.5$  mm) and the fact that measurements made on the operating characteristics of the  $^3\text{He}$  refrigerator indicate that only about three-quarters of the  $^3\text{He}$  is in the form of liquid in the sample tube, it was still felt that an independent check should be made. This was accomplished by operating the refrigerator with only 1.2 liter (NTP) of  $^3\text{He}$  in the system. Under these conditions, one has to wait slightly longer than normally for the sample to cool down each time it is replaced in the  $^3\text{He}$  liquid. The results of these measurements are given in Sec. IVB.

There could also be an increase or decrease in the cross section if holmium metal had an abnormally large expansion coefficient. Although there is no reason to believe this, there have been very few measurements made for metals in general in this temperature region ( $4.2$  to  $0.33^\circ\text{K}$ ), and in fact none for any of the rare-earth metals. In order to check this point as well as the possibility of other systematic errors, a series of transmission measurements was made on a "dummy" holmium sample. This sample was cut out of a polycrystalline rod of holmium metal into the same shape and mounted in the cryostat in the same way as the single crystal. Because of the polycrystalline structure of this sample there can be no net nuclear alignment at any temperature. Transmission measurements were made at  $4.2$  and  $0.33^\circ\text{K}$  in exactly the same way as those made on the single crystal. The results of these measurements are also discussed in Sec. IVB.

### III. NUCLEAR ALIGNMENT OF $^{165}\text{Ho}$

The first two nuclear-orientation parameters<sup>24</sup>  $f_1$ , (nuclear polarization) and  $f_2$ , (nuclear alignment) have been calculated for  $^{165}\text{Ho}$  when it is in the form of a metal single crystal.<sup>6</sup> Since we are only concerned with nuclear alignment in these measurements, we will quickly review the information which goes into calculating this quantity. The explicit form for the nuclear-alignment parameter  $f_2$  is

$$f_2 = I^{-2} \left[ \sum_m m^2 P_m - I(I+1)/3 \right], \quad (1)$$

<sup>24</sup> H. A. Tolhoek and J. A. M. Cox, *Physica* **19**, 101 (1953); actually all of the odd parameters are called polarization parameters and all of the even ones alignment parameters.

where  $I$  is the nuclear spin and the  $P_m$  are the occupational probabilities of the different magnetic substates  $m$ .

Although holmium metal has one of the largest hyperfine interactions known,<sup>25</sup> and at first sight seems to be an ideal target for nuclear orientation experiments, a closer look at its atomic magnetic properties reveals unexpected complications. The low-temperature neutron-diffraction data of Koehler *et al.*,<sup>26</sup> for a single crystal of holmium metal, in the absence of a magnetic field, indicate that the atomic moments are canted out of the basal plane of the hcp crystal lattice by a small angle and give rise to a ferromagnetic spiral spin structure.<sup>27</sup> The axis of this spin structure is parallel to the  $c$  axis of the crystal. Since the canting angle is small, the larger component of the magnetic moment lies in the basal plane and is antiferromagnetic. The smaller component along the  $c$  axis is ferromagnetic.<sup>28</sup> If we subdivide the atomic system of the crystal into groups whose atomic moments lie along a particular axis, then fairly large values of nuclear alignment can be obtained in the neighborhood of  $0.3^\circ\text{K}$  for each of these groups relative to its common axis.<sup>29</sup> These axes (there are perhaps twelve of them) lie close to the basal plane. This degeneracy (of having more than one alignment axis) can be removed by lining up the atomic moments with a magnetic field. For a field applied along an easy direction of magnetization, and for a favorably shaped sample, only a few kOe is needed.<sup>30</sup> In the presence of a field we thus not only have an aligned target, but a polarized target as well. However, in the present experiment we were not interested in polarization effects and only required nuclear alignment. Since we restricted ourselves to a total-cross-section measurement, we did not have to remove the degeneracy of many alignment axes in the basal plane as long as this plane was perpendicular to the beam direction.

The value of  $f_2$  can be readily calculated for any one of these groups with respect to its common axis. The

<sup>25</sup> V. B. Belionin, *Opt. i Spectroskopiya* **5**, 236 (1958); J. E. Gordon, C. W. Dempsey, and T. Soller, *Phys. Rev.* **124**, 724 (1961); H. Postma, H. Marshak, V. L. Sailor, F. J. Shore, and C. A. Reynolds, *ibid.* **126**, 979 (1962); B. Bleaney, *J. Phys. Soc. Japan* **17**, suppl. B1, 435 (1962); O. V. Lounasmaa, *Phys. Rev.* **128**, 1136 (1962); H. V. Kempen, A. R. Miedema, and W. J. Huiskamp, *Physica* **30**, 229 (1964); G. Brunhart, H. Postma, and V. L. Sailor, *Phys. Rev.* **137**, B1484 (1965).

<sup>26</sup> W. C. Koehler, J. W. Cable, E. O. Wollan, and M. K. Wilkinson, *J. Phys. Soc. Japan* **17**, Suppl. B-III, 32 (1962); W. C. Koehler, *J. Appl. Phys.* **36**, 1078 (1965).

<sup>27</sup> At  $4.2^\circ\text{K}$ , the atomic moments seem to be grouped about the six directions of easy magnetization ( $b$  axes) of the crystal rather than have one definite turn angle; see W. C. Koehler, *J. Appl. Phys.* **36**, 1078 (1965).

<sup>28</sup> In the virgin magnetic state there is, of course, no net moment along the  $c$  axis of the crystal due to the existence of mirror image domains.

<sup>29</sup> Although this method of nuclear alignment is somewhat similar to the Bleaney method it should really be credited to Dr. C. P. Bean; see M. A. Grace, C. E. Johnson, N. Kurti, R. G. Scurlock, and R. T. Taylor, *Phil. Mag.* **4**, 948 (1959).

<sup>30</sup> D. L. Strandburg, S. Legvold, and F. H. Spedding, *Phys. Rev.* **127**, 2046 (1962); D. L. Strandburg, thesis, Iowa State University, 1962 (unpublished).

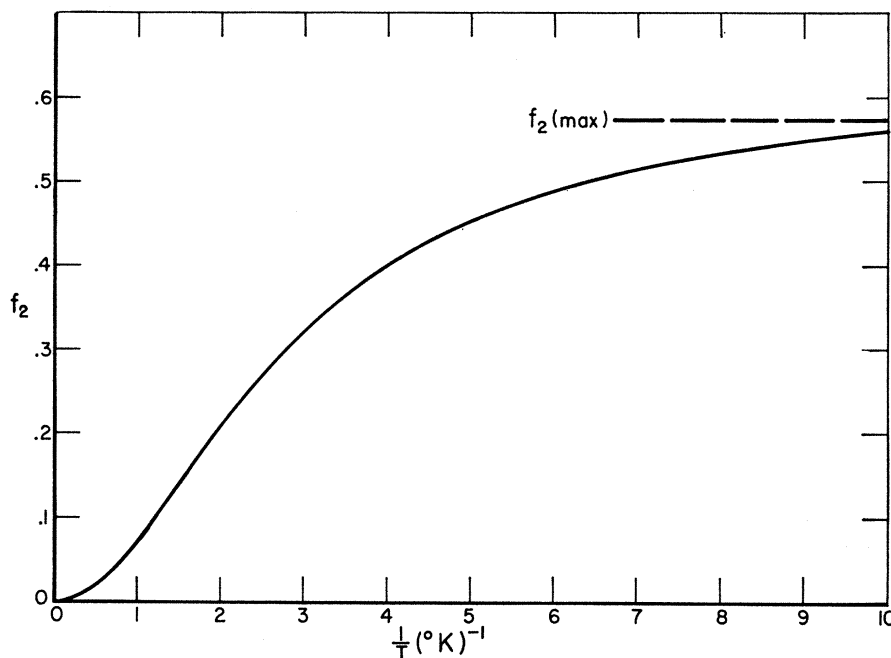


FIG. 8. Nuclear orientation parameter  $f_2$  for  $^{165}\text{Ho}$  as a function of the reciprocal of the temperature. This parameter was calculated for the group of holmium nuclei, in a single metal crystal, whose atomic moments lie along a common axis (see text).

hyperfine field at the nucleus ( $\sim 9 \times 10^6$  Oe) removes the spin degeneracy, that is, splits the ground-state spin ( $I = \frac{7}{2}$  for  $^{165}\text{Ho}$ ) into  $2I+1$  equally spaced magnetic sublevels. Since the hyperfine coupling constant is positive for  $^{165}\text{Ho}$ , the lowest magnetic substate is  $+\frac{7}{2}$ . We have a manifold of eight equally spaced levels going from  $+\frac{7}{2}$  to  $-\frac{7}{2}$ . With respect to the common axis of the group there are as many atomic moments parallel as antiparallel; therefore we have as many manifolds going from  $-\frac{7}{2}$  to  $+\frac{7}{2}$  as from  $+\frac{7}{2}$  to  $-\frac{7}{2}$ . We can thus picture the group as having a pattern of eight equally spaced hyperfine doublets with quantum numbers  $\pm m$ . This situation can be represented by using a fictitious spin Hamiltonian with effective spin  $S = \frac{1}{2}$  to represent the system, viz.,

$$\mathcal{H} = AI_z S_z, \quad (2)$$

where  $A$  is the hyperfine coupling constant and  $I_z$  and  $S_z$  are the spin operators with respect to the group's common axis,  $z$ . The energy levels for this Hamiltonian are

$$E_m = \pm \frac{1}{2} Am. \quad (3)$$

The occupational probabilities  $P_m$  can be directly calculated using the Boltzmann factor. The resulting expression for  $f_2$  is

$$f_2 = I^{-2} \left[ \frac{\sum_m m^2 e^{Am/2kT}}{\sum_m e^{Am/2kT}} - \frac{1}{3} I(I+1) \right]. \quad (4)$$

This quantity was calculated for the relevant temperature region and using a value of  $0.62^\circ\text{K}$  for  $A/k$  (see Fig. 8.). The occupational probabilities are given in Table I for the temperature used in our measurements ( $0.33^\circ\text{K}$ ).

Since the alignment axes are really not in the basal plane, the value for the nuclear alignment parameter

( $f_2 = 0.32$  at  $0.33^\circ\text{K}$ ) referred to the axis projected in the basal plane is slightly reduced. This reduction in  $f_2$  can be calculated by using the appropriate rotation matrix,  $D_{00}^2(\theta) = P_2(\cos\theta)$ . The canting angle ( $\theta \approx 10^\circ$ ) is obtained from neutron diffraction<sup>26</sup> and magnetization data.<sup>30</sup> For this angle the reduction in  $f_2$  is about 4%. There are several effects which will introduce small uncertainties into the value of  $f_2$ , namely, the error in the canting angle, misalignment of the  $c$  axis of the crystal with respect to the neutron beam direction (see Sec. IIb), the small error in the temperature measurement ( $\pm 10$  mdeg), the inclusion of a small quadrupole term<sup>31</sup> in the spin Hamiltonian, and the possibility of a higher value for the hyperfine coupling constant ( $A/k = 0.64^\circ\text{K}$ ).<sup>31</sup> This last item would increase  $f_2$  by a few percent. When all these effects are taken into account, the value of  $f_2$  for our measurements is  $0.31 \pm 0.02$ .

#### IV. EXPERIMENTAL PROCEDURE AND RESULTS

##### A. The Total Neutron Cross Section of $^{165}\text{Ho}$

Two cylindrical polycrystalline samples<sup>32</sup> (1.259 cm and 3.340 cm thick) were prepared from a single ingot of 99.9% pure holmium metal. The measured density was  $8.82 \text{ g/cm}^3$  and radiographs showed an absence of voids. Each of the samples was positioned by a low-mass holder with its cylindrical axis lying along the neutron beam and with its face 7.12 cm from the target.

<sup>31</sup>H. Van Kempen, A. R. Miedema, and W. J. Huiskamp, *Physica* **30**, 229 (1964).

<sup>32</sup>We are grateful to J. Johnson of Oak Ridge National Laboratory for lending us these holmium samples.

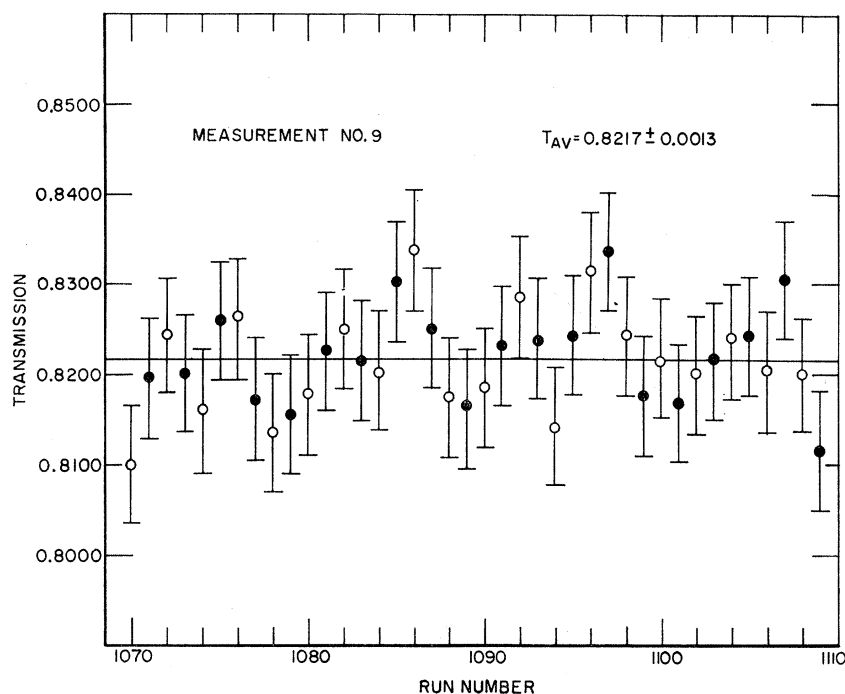


FIG. 9. A typical transmission measurement. The errors shown on the individual transmission points are those due to counting statistics. The solid line is the arithmetic mean ( $T_{av}$ ) and the error given is the standard deviation of this mean.

At this distance the neutron beam was well inside the edges of the 2.17-cm diam. samples. The neutron detector was located in the same position (25.6 cm) as for the alignment measurements. This geometry is not optimal for a transmission measurement. The in-scattering correction amounted to 14.0% and 15.7% of the total cross section for the thin and thick samples, respectively. The resulting uncertainty in the final value of the total cross section was about 2% because of this correction. This geometry was tolerated because it was required for measurement of the alignment effect, and a more accurate measurement of  $\sigma_t$  was not needed in view of the uncertainty in the measured change in the cross section due to nuclear alignment. The formula used for calculating the in-scattering correction is derived in the Appendix and includes the effects of both sample and detector thickness.

The results of the transmission measurements on these samples are shown in Table II. Two sample thicknesses were employed, one roughly the  $^{165}\text{Ho}$  single-crystal thickness and the other (thicker) providing a check on the in-scattering calculation. The procedures used for collection and reduction of these data were the same as those detailed in Sec. IVB. The errors shown for the transmission values are the standard deviations of the

TABLE I. Occupational probabilities of the nuclear magnetic substates for  $^{165}\text{Ho}$ , for  $T=0.33^\circ\text{K}$  and  $A/k=0.62^\circ\text{K}$ . These were calculated for the group of nuclei whose atomic moments lie along a common axis (see text).

| $m$   | $\pm\frac{7}{2}$ | $\pm\frac{5}{2}$ | $\pm\frac{3}{2}$ | $\pm\frac{1}{2}$ | $\mp\frac{1}{2}$ | $\mp\frac{3}{2}$ | $\mp\frac{5}{2}$ | $\mp\frac{7}{2}$ |
|-------|------------------|------------------|------------------|------------------|------------------|------------------|------------------|------------------|
| $P_m$ | 0.305            | 0.120            | 0.049            | 0.025            | 0.025            | 0.049            | 0.120            | 0.305            |

experimental data; those for the cross sections include the uncertainty in the in-scattering correction as well. Uncertainties due to sample impurity, density, and thickness are all negligibly small. The final value for the total cross section was obtained in the usual manner: by weighting the values for the two samples by the inverse square of their errors.

#### B. The Effect of Nuclear Alignment on $\sigma_t$

Transmission of the  $^{165}\text{Ho}$  single crystal cooled to  $0.33^\circ\text{K}$  ( $f_2=0.31$ ) and  $4.2^\circ\text{K}$  ( $f_2=0.005$ ) was measured as described in Sec. II. Ten such measurements were made; four at  $4.2^\circ\text{K}$ , four at  $0.33^\circ\text{K}$ , and two additional

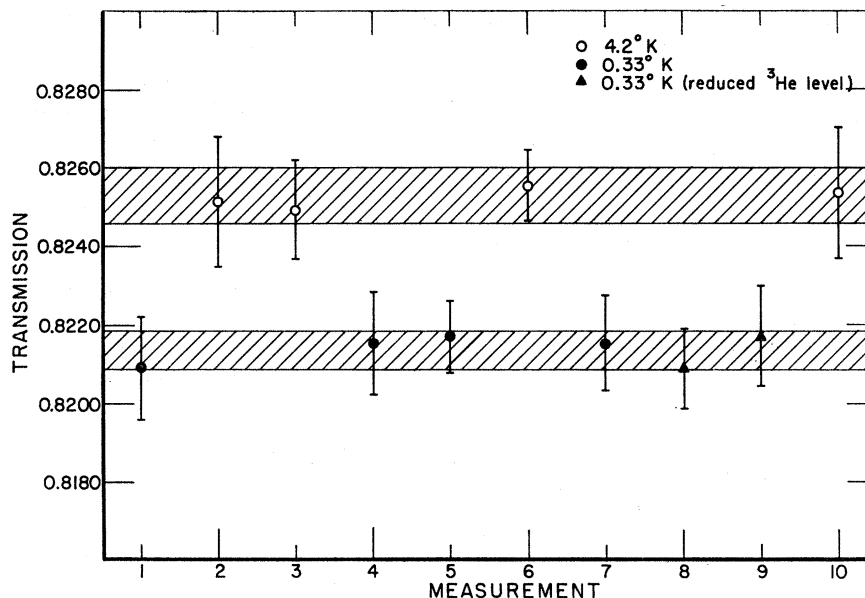
TABLE II. Results of the transmission measurements on un-oriented  $^{165}\text{Ho}$ . These measurements were carried out at room temperature using polycrystalline samples and under the same beam and detector conditions as those used for the cryogenic target.

| Measurement No. | Transmission <sup>a</sup> |                     |
|-----------------|---------------------------|---------------------|
|                 | $t=1.259$ cm              | $t=3.340$ cm        |
| 1               | $0.8289 \pm 0.0011$       |                     |
| 2               |                           | $0.6198 \pm 0.0009$ |
| 3               | $0.8324 \pm 0.0009$       |                     |
| 4               | $0.8330 \pm 0.0010$       |                     |
| 5               |                           | $0.6196 \pm 0.0011$ |
| 6               | $0.8310 \pm 0.0012$       |                     |
| Weighted mean   | $0.8313 \pm 0.0005$       | $0.6197 \pm 0.0007$ |
| $\sigma_t(b)^b$ | $5.30 \pm 0.09$           | $5.28 \pm 0.11$     |
| Average         | $5.29 \pm 0.10$           |                     |

<sup>a</sup> These data have been corrected for background only. The errors quoted are the standard deviation of the mean.

<sup>b</sup> These results have been corrected for in-scattering. Most of the error in the final result is due to this correction. Since the in-scattering correction is approximately the same for both sample thicknesses, the error associated with the average value is only slightly reduced.

FIG. 10. Transmission measurements for the  $^{165}\text{Ho}$  single crystal. The errors shown on the individual transmission measurements are standard deviations of the mean. The shaded areas represent the standard deviations of the weighted averages of the measurements at 0.33 and 4.2°K.



measurements at 0.33°K with reduced  $^3\text{He}$  level (Sec. IIB). Finally the single crystal was replaced by the polycrystalline “dummy” sample and five additional transmission measurements were made at the same two temperatures ( $f_2=0$  at both 0.33 and 4.2°K). These data were taken over three periods of several days each of continuous running, alternating, in a random way, 0.33 and 4.2°K measurements.

Each transmission measurement was made up of forty-one consecutive 10-min runs, with the sample alternately in and out of the beam. Figure 9 shows the runs comprising a typical measurement. The data showed no systematic trends and exhibited the 0.1% reproducibility from measurement to measurement consistent with the total number of counts recorded, which was typically  $10^6$ . The background for each 10-min run was determined by extrapolating the number of

counts in the region of the time spectrum indicated on Fig. 5 to the entire range of fast-coincidence-time response. It was found that the final value for a transmission measurement was insensitive to the exact region of the time spectrum chosen for this extrapolation. The transmission value for each measurement is taken to be the arithmetic mean of the transmissions calculated for each of the 40 consecutive pairs of runs. The error is the standard deviation (not just the error expected from counting statistics), but considering only 20 pairs of runs to be statistically independent.

The single-crystal results are shown in Fig. 10 and in Table III. It can be seen that reducing the  $^3\text{He}$  level had no effect on the measured transmission; these results were therefore included in determining the size of the alignment effect. The fractional change in the total cross section,  $\Delta\sigma_t/\sigma_t$ , due to nuclear alignment is given by

$$\frac{\Delta\sigma_t}{\sigma_t} = \frac{\sigma_{t,a} - \sigma_t}{\sigma_t} = \frac{\ln(T/T_a)}{\ln(1/T) - (Nt\sigma)_{\text{Cu}}}, \quad (5)$$

where  $\sigma_{t,a}$  and  $T_a$  are the total cross section and transmission ratio, respectively, for the aligned target;  $T$  is the unaligned transmission ratio;  $N$ ,  $t$ , and  $\sigma$  are the nuclear density, thickness, and 14-MeV total neutron cross section, respectively, for two thin copper plates used to hold the  $^{165}\text{Ho}$  single crystal in its mounting basket in the cryostat. These copper plates moved in and out of the neutron beam with the single crystal. The measured transmissions  $T$  and  $T_a$  were corrected for in-scattering. The angular distribution for the aligned target was calculated using our value of  $f_2$  and the same optical-model parameters as those used for the unaligned angular distribution. This correction increases the effect by a small amount (see Appendix). The resulting value

TABLE III. Results of the transmission measurements on aligned  $^{165}\text{Ho}$ .

| Measurement No. | Transmission <sup>a</sup>                |  |
|-----------------|--|--|
|                 | $T=0.33^\circ\text{K}$<br>( $f_2=0.31$ ) | $T=4.2^\circ\text{K}$<br>( $f_2=0.005$ ) |
| 1               | 0.8209±0.0013                            |  |
| 2               |  | 0.8251±0.0017                            |
| 3               |  | 0.8249±0.0012                            |
| 4               | 0.8214±0.0013                            |  |
| 5               | 0.8217±0.0009                            |  |
| 6               |  | 0.8255±0.0009                            |
| 7               | 0.8215±0.0012                            |  |
| 8 <sup>b</sup>  | 0.8209±0.0010                            |  |
| 9 <sup>b</sup>  | 0.8217±0.0013                            |  |
| 10              |  | 0.8253±0.0017                            |
| Weighted mean   | 0.8214±0.0005                            | 0.8253±0.0007                            |

<sup>a</sup> These data have been corrected for background only. Corrections for in-scattering and the copper plates retaining the crystal have not been made to these data (see text for these corrections). The errors quoted are the standard deviation of the mean.

<sup>b</sup> Reduced  $^3\text{He}$  level.

TABLE IV. Results of the transmission measurements on polycrystalline  $^{165}\text{Ho}$ .

| Measurement No. | Transmission <sup>b</sup>                |   |
|-----------------|--|---|
|                 | $T=0.33^\circ\text{K}$<br>( $f_2=0.00$ ) | $T=4.2^\circ\text{K}$<br>( $f_2=0.00$ ) |
| 11              | 0.8229±0.0010                            |   |
| 12              |  | 0.8225±0.0014                           |
| 13              | 0.8243±0.0008                            |   |
| 14              | 0.8211±0.0012                            |   |
| 15              |  | 0.8242±0.0011                           |
| Weighted mean   | 0.8231±0.0006                            | 0.8235±0.0009                           |

<sup>a</sup> This sample was nearly identical in shape and size to the single crystal sample.

<sup>b</sup> The errors quoted are the standard deviation of the mean.

for (5) is

$$\Delta\sigma_t/\sigma_t = +(3.52 \pm 0.75)\% \quad (6a)$$

Using the value for  $\sigma_t$  given in Table II, we obtain (for our value of nuclear alignment)

$$\Delta\sigma_t = +(186 \pm 40)\text{mb}, \quad (6b)$$

where the positive sign indicates a larger cross section for nuclei aligned perpendicular to the incident beam than for randomly oriented nuclei.

The results for the polycrystalline "dummy" sample are shown in Table IV. These results indicate the apparent absence of any systematic influences on the measured alignment effect for the temperature change from 0.33 to 4.2°K. The quoted uncertainty in the nuclear

alignment effect is thus due mainly to the standard deviations of the transmission measurements, with small contributions from the error in the total cross section, the inscattering correction, and the correction for the copper plates retaining the single crystal.

## V. THEORETICAL ANALYSIS

### A. Coupled-Channel Calculations

Our previous data on the scattering of 350-keV neutrons by oriented  $^{165}\text{Ho}$  were analyzed and fitted successfully<sup>6</sup> in terms of the nonadiabatic coupled-channel calculations (NACC).<sup>8</sup> Since the energy of the neutrons (14 MeV) used in the present experiment is much larger than the rotational energy of the target ( $\sim 100$  keV), the adiabatic coupled-channel calculation (ACC)<sup>8</sup> can be used with a high degree of accuracy. The use of ACC also makes<sup>8</sup> the machine time for the computation comparatively short, in spite of the fact that a much larger number of partial waves has to be taken into account this time compared to that in our previous analysis.

Since the derivation of the adiabatic coupled-channel equations and their solutions, in the form of the scattered waves and the cross sections, have been presented in detail<sup>33</sup> in Sec. V of T, and the results are just quoted here. The expression for the total cross section,  $\sigma_t$ , is found in (T-53) if the quantity  $Z_{m_s M_1, m_s' M_1'; \nu}$  of (T-52) that appears there is replaced by  $Z_{m_s M_1, m_s' M_1'; \nu}^{(\text{ACC})}$  of (T-72). Thus

$$\sigma_t^{(\text{ACC})} = (4\pi/k_1^2) \sum_{l'} (2l'+1) \text{Im} \sum_{ii' m_s m_s' M_1 M_1'} a_{m_s}^{(i)} a_{m_s}^{(i')} b_{M_1}^{(i')} b_{M_1'}^{(i')} Z_{m_s M_1, m_s' M_1'; \nu}^{(\text{ACC})}. \quad (7)$$

Unfortunately there was a slight error in (T-72) and the following is the correct expression for  $Z_{m_s M_1, m_s' M_1'; \nu}^{(\text{ACC})}$ :

$$Z_{m_s M_1, m_s' M_1'; \nu}^{(\text{ACC})} = \sum_{j l j' m_j m_j'} (l s 0 m_s | j m_s) (l' s 0 m_s' | j' m_s') (-)^{m_s' - \bar{m}_j} C_{l j \nu j' \bar{m}_j} \times \sum_{J M_J} (I_1 J K 0 | I_1 K) (I_1 J M_1 M_J | I_1 M_1') (j j' \bar{m}_j - \bar{m}_j | J 0) (j j' m_s - m_s' | J M_J). \quad (8)$$

All the notations in (7) and (8) are the same as in T. In particular, the meaning and derivation of the coefficients  $a_{m_s}^{(i)}$  and  $b_{M_1}^{(i')}$  in (7), which describe the orientation and/or polarization of the projectile and the target, respectively, have been explained in detail in T and Ref. 6. Moreover, the orientation of the target in the present experiment and thus the description of  $a_{m_s}^{(i)}$  and  $b_{M_1}^{(i')}$  are exactly the same as in Ref. 6.

Since the experimental datum to be fitted is only  $\sigma_t$ , and no differential scattering cross section<sup>34</sup>  $\sigma(\theta, \varphi)$  is available, Eqs. (7) and (8) seem to suffice for the fitting. In deriving the experimental value of the total cross section (which was given in Table II, and will henceforth be called  $\sigma_t^{(\text{expt})}$ ) however, we had to perform the inscattering corrections and for that purpose we have to know  $\sigma(\theta, \varphi)$ .

The general expression for the differential cross section,  $\sigma(\theta, \varphi)$ , can be found in (T-49) by replacing  $X_{m_s M_1, m_s' M_1'}(\theta, \varphi)$  of (T-48) by  $X_{m_s M_1, m_s' M_1'}^{(\text{ACC})}(\theta, \varphi)$  of (T-71).<sup>35</sup> As was emphasized in T,  $\sigma(\theta, \varphi)$  is in general dependent on the azimuthal angle  $\varphi$  as well as the polar angle  $\theta$ . The angular distribution  $\sigma(\theta)$  which we need in the inscattering correction is, however, not  $\sigma(\theta, \varphi)$ , but  $\sigma(\theta, \varphi)$  averaged over  $\varphi$ . This is due to the fact that our detector is set in a cylindrically symmetric way with respect to the incident beam which has been chosen as the  $z$  axis of our quantization.

<sup>33</sup> Reference 8 will be referred to as T in the following. Equations in T will be referred to by adding T to the number of that equation; e.g., (T-53).

<sup>34</sup> Here and in the following we will consider only the elastic scattering differential cross section. Therefore the cross section  $\sigma_n(\theta, \varphi)$  ( $n=1$  for the elastic scattering) defined in (T-49) will be used without subscript  $n$ .

<sup>35</sup> In the second line of (T-71) the factor  $l'$  is to be read  $\bar{l}'$ . In the following we shall write  $M_1'$  for  $M_n$ .

The expression  $\sigma(\theta, \varphi)$  for elastic scattering is given by [cf. (T-49)]

$$\sigma(\theta, \varphi) = \sum_{ii'm_s'M_1'} \left| \sum_{m_s M_1} X_{m_s M_1 m_s' M_1'}^{(\text{ACC})}(\theta, \varphi) a_{m_s}^{(i)} b_{M_1}^{(i')} \right|^2, \quad (9)$$

with

$$X_{m_s M_1 m_s' M_1'}^{(\text{ACC})}(\theta, \varphi) = \sum_{ljl'j'\bar{m}_j m_l' m_j'} [(4\pi)^{1/2}/k_1] \hat{l}' C_{lj l' j'} \bar{m}_j (l s 0 m_s | j m_s) \sum_{JM_J} (-)^{\bar{m}_j - m_j'} (I_1 J K 0 | I_1 J K) \\ \times (I_1 J M_1 M_J | I_1 M_1') (j j' \bar{m}_j - \bar{m}_j | J 0) (j j' m_s - m_s' | J M_J) (l' s m_s' | j' m_j') Y_{l' m_l'}(\theta, \varphi). \quad (10)$$

Equation (10) is simpler than (T-71) since it is restricted to the elastic scattering of chargeless projectiles.

In order to obtain

$$\sigma(\theta) = \frac{1}{2\pi} \int_0^{2\pi} \sigma(\theta, \varphi) d\varphi, \quad (11)$$

we first note that the  $\varphi$  dependence of  $\sigma(\theta, \varphi)$  is only through  $Y_{l' m_l'}(\theta, \varphi)$  and that the  $\varphi$  dependence of  $Y_{l' m_l'}(\theta, \varphi)$  is only through a factor  $\exp[im_l' \varphi]$ . We further note the following obvious relation:

$$\frac{1}{2\pi} \int_0^{2\pi} [\exp(im_l' \varphi)]^* [\exp(im_l' \varphi)] d\varphi = \delta_{m_l' m_l'}.$$

Because of these facts it is easy to see that  $\sigma(\theta)$  is expressed by (9) using the same expression (10) for  $X_{m_s M_1 m_s' M_1'}^{(\text{ACC})}(\theta, \varphi)$ , except that the summation over  $m_l'$  in the right-hand side of (10) is suppressed and a summation over  $m_l'$  is added in (9) outside the square symbol. In other words, if we understand that a symbol  $X_{m_s M_1 m_s' M_1'; m_l'}^{(\text{ACC})}(\theta, \varphi)$  means the quantity on the right-hand side of (10) after the summation over  $m_l'$  is suppressed, we get  $\sigma(\theta)$  as

$$\sigma(\theta) = \sum_{ii'm_s'M_1' m_l'} \left| \sum_{m_s M_1} X_{m_s M_1 m_s' M_1'; m_l'}^{(\text{ACC})}(\theta, \varphi) a_{m_s}^{(i)} b_{M_1}^{(i')} \right|^2. \quad (12)$$

It is clear that the dependence of the right-hand side of (12) on  $\varphi$  is only apparent.

Equation (12) is correct but may be somewhat misleading. The reason is that the summation over  $m_l'$  in (10) is redundant since  $m_l'$  must always be equal to  $m_s + M_1 - m_s' - M_1'$ . Therefore what is meant by the appearance of the summation over  $m_l'$  outside the square symbol in (12) is that the summations over  $m_s$  and  $M_1$  inside the square symbol are not independent but are restricted by the condition that  $m_s + M_1 = m_s' + M_1' + m_l'$ . Thus the meaning of (12) will become clearer if it is written, by introducing a Kronecker symbol  $\delta_{m_s + M_1, m_s' + M_1' + m_l'}$ , as

$$\sigma(\theta) = \sum_{ii'm_s'M_1' m_l'} \left| \sum_{m_s M_1} \delta_{m_s + M_1, m_s' + M_1' + m_l'} X_{m_s M_1 m_s' M_1'; m_l'}^{(\text{ACC})}(\theta, \varphi) a_{m_s}^{(i)} b_{M_1}^{(i')} \right|^2. \quad (13)$$

The somewhat complicated argument made in deriving (13) was forced on us because we wanted to make the evaluation of  $\sigma(\theta)$  as close to that of  $\sigma(\theta, \varphi)$  as possible. Indeed, the evaluation of (13) by the computer required only a very slight modification to the part of the program that was already coded for the evaluation of (9).

The argument might have been much simpler if the square had been taken in (9), with (10), and the summation over magnetic quantum numbers was performed analytically. In the machine calculation, however, this method is to be avoided, since then the machine time needed to evaluate  $\sigma(\theta, \varphi)$  becomes formidably long, a point which was already made in T (cf. Ref. 21 of T).

In our previous analysis<sup>6</sup> it was found that the simultaneous fit of  $\sigma(\theta, \varphi)$ ,  $\sigma_t$  and  $\Delta\sigma_t$  narrows down the possible sets of allowed optical model parameters very nicely. As was mentioned above, we do not have data for  $\sigma(\theta, \varphi)$  this time. This makes the data fitting, namely, the search of the optical-model parameters, comparatively easy, though the set of parameters found by fitting  $\sigma_t$

and  $\Delta\sigma_t$  might have to be changed slightly in order to also fit  $\sigma(\theta, \varphi)$ .

The numerical calculations were performed by using the CDC-1604 computer at Oak Ridge. Because of the simplicity of the present analysis, as mentioned in the preceding paragraph, a few production runs, each run taking about 15 min, were sufficient to obtain a set of parameters that make the theoretical values of  $\sigma_t$  and  $\Delta\sigma_t$  fit the corresponding experimental values within their experimental errors. The meaning of the optical-model parameters is the same as in T and Ref. 6, and we list here their values without explanation:

$$V=46.0, \quad W=0, \quad W_D=7.5, \quad V_{so}=7.5 \quad (\text{all in MeV}), \\ r_0=\bar{r}_0=1.25, \quad a=0.65, \quad \bar{a}=0.47 \quad (\text{all in F}), \quad (14) \\ \beta=0.30.$$

With these parameters, which are the same as those used in WMTM except for  $V$  and  $W_D$ , we get

$$\sigma_t^{(\text{ACC})}(\text{unoriented}) = 5.296b \\ \text{and} \quad \Delta\sigma_t/\sigma_t = 3.32\% \quad (15)$$

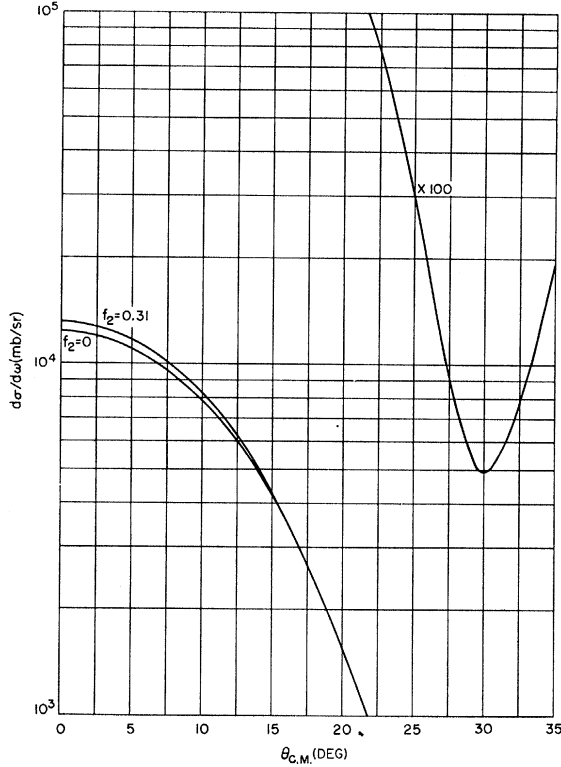


FIG. 11. Theoretical angular distributions for unaligned nuclei ( $f_2=0$ ) and for aligned nuclei ( $f_2=0.31$ ) using an adiabatic coupled-channel calculation. The optical-model parameters used were the same as those used to fit the measured total cross section and the deformation effect. The  $f_2=0.31$  curve is  $\sigma(\theta)$  defined in (13) of the text.

which are in complete agreement with experimental values given in Table II and Eq. (6.1), respectively.

As was mentioned above,  $\sigma(\theta)$  of Eq. (13) had to be known in order to obtain the inscattering corrections. Since a set of optical model parameters that gives a certain value of  $\sigma(\theta)$  then determines  $\sigma_i(\text{exp}^t)$ , which in turn has to be fitted by the above given set of parameters, the data-fitting procedure has been a little more complicated than was explained above. Indeed, we had to fit  $\sigma(\theta)$ , in addition to  $\sigma_i$  and  $\Delta\sigma_i$ , in spite of the fact that  $\sigma(\theta)$  was not measured directly. With slight changes of parameters that give reasonable values for  $\sigma_i$  and  $\Delta\sigma_i$  (that are not very far from our experimental results), the difference of the inscattering correction due to changes of  $\sigma(\theta)$  was rather small, and thus the simultaneous fit of three quantities,  $\sigma(\theta)$ ,  $\sigma_i$ , and  $\Delta\sigma_i$  was carried out without too much difficulty.

In order to give an idea of how  $\sigma(\theta)$  differs for oriented and unoriented targets, we show in Fig. 11 its values obtained with the parameters as given in Eq. (14).

### B. Black-Nucleus Model

Although the wavelength of a 14-MeV neutron is only about equal to the radius (for a deformed nucleus we use

for the radius,  $R$ , that of a spherical nucleus of equal volume) of the holmium nucleus, and therefore the black-nucleus model (which requires  $kR \gg 1$ ) is not yet valid, it is still instructive to calculate the quantity  $\Delta\sigma_i/\sigma_i$  in terms of it. The general formalism has been developed by Visotskii *et al.*,<sup>2</sup> and the results for various values of  $a/b$  ( $2a$  is the length of the symmetry axis of the ellipsoid of revolution and  $2b$  is the diameter of the largest circular cross section) are given for complete nuclear alignment. The relevant equation for  $\Delta\sigma_i/\sigma_i$  can, however, be derived in a more straightforward manner than that in Visotskii *et al.*, and in such a way that the effect of nuclear alignment shows up directly in the resulting expression.<sup>36</sup>

For simplicity we shall only derive the expression for the case where the spin-density matrix  $\rho$  is diagonal; that is, where we have axially symmetric nuclear orientation. In this case the total cross section  $\sigma_i$  can be written as

$$\sigma_i = \sum_{m=-I}^I \rho_{mm} \sigma_{im}^I = \sum_m P_m \sigma_{im}^I, \quad (16)$$

where  $\rho_{mm}$  is a diagonal element of the density matrix and is equal to  $P_m$ , the population of the magnetic substate  $m$  of the target nucleus with spin  $I$ . The quantity  $\sigma_{im}^I$  is the total cross section associated with each of the  $m$  states. Using the Fraunhofer approximation, the total cross section associated with each of the  $m$  states for a rotational nucleus,  $\sigma_{imK}^I$ , is given by [Eq. (14), Ref. 2]

$$\sigma_{imK}^I = \frac{2\pi(2I+1)R^2}{(1+\epsilon)^{1/3}} (-)^{m-K} \sum_{L=0}^{2I} (II m - m | L 0) \times (II K - K | L 0) P_L(\cos\psi) A_L, \quad (17)$$

where  $R$  has been defined before,  $\epsilon = (a/b)^2 - 1$ ,  $\psi$  is the angle between the wave vector of the incident neutron and the orientation axis,  $K$  is the projection of  $I$  along the symmetry axis, and  $A_L$  is given by

$$A_L = \frac{1}{2} \int_0^\pi [1 + \epsilon \sin^2\vartheta]^{1/2} P_L(\cos\vartheta) \sin\vartheta d\vartheta, \quad (18)$$

where  $\vartheta$  is the angle between the symmetry axis of the nucleus and the wave vector of the scattered neutron. The integrals given by  $A_L$  vanish for  $L$  odd, and therefore we only have to retain the terms even in  $L$ .

Putting (17) into (16) we obtain

$$\sigma_i = \frac{2\pi(2I+1)R^2}{(1+\epsilon)^{1/3}} (-1)^{I-K} \sum_{L \text{ even}} (II K - K | L 0) \times P_L(\cos\psi) A_L \sum_m P_m (-1)^{m-I} (II m - m | L 0), \quad (19)$$

<sup>36</sup> This method is somewhat similar to that used in Ref. 5.

where the phase factor  $(-1)^{m-K}$  has been replaced by  $(-1)^{I-K}(-1)^{m-I}$ . The summation over  $m$  is just the nuclear orientation parameter  $\bar{f}_L$ .<sup>24,37</sup> These parameters are related to the more familiar orientation parameters  $f_L$  (those used in Sec. III) by the equation

$$\bar{f}_L = \binom{2L}{L} I^L \left[ \frac{(2L+1)(2I-L)!}{(2I+L+1)!} \right]^{1/2} f_L. \quad (20)$$

In terms of  $\bar{f}_L$ , (19) can be written

$$\sigma_t = \frac{2\pi(2I+1)R^2}{(1+\epsilon)^{1/3}} (-1)^{I-K} \sum_{L \text{ even}} (IIK-K|L0) P_L(\cos\psi) A_L \bar{f}_L. \quad (21)$$

The fractional change in the average total cross section due to nuclear alignment, which is the quantity we need to compare this model to our experimental results, is given by the following relation:

$$\frac{\Delta\sigma_t}{\sigma_t} = \frac{P_2 A_2 \bar{f}_2 (IIK-K|20)}{A_0 \bar{f}_0 (IIK-K|00)} + \frac{P_4 A_4 \bar{f}_4 (IIK-K|40)}{A_0 \bar{f}_0 (IIK-K|00)} + \dots \quad (22)$$

Calculations made for <sup>165</sup>Ho, which is one of the most highly deformed rotational nuclei ( $\beta=0.30$ ,  $a/b=1.31$ ), and for the limiting case of complete nuclear alignment ( $m=\pm\frac{1}{2}$  only) perpendicular to the incident beam ( $\psi=\pi/2$ ), show that the  $L=6$  term is completely negligible and the  $L=4$  term contributes less than 1% to the total effect. The result for our value of nuclear alignment ( $f_2=0.31$  and  $f_4=0.013$ ) and geometry is

$$\Delta\sigma_t/\sigma_t = +2.13\%, \quad (23)$$

This is considerably lower than our measured value:  $(+3.52 \pm 0.75)\%$ ; and that predicted by ACC:  $+3.32\%$ .

## VI. CONCLUSIONS

As we have seen in Sec. VA, our experimental results for  $\sigma_t$  and  $\Delta\sigma_t/\sigma_t$  were fitted very well by the coupled-channel calculation. Although we did not have the experimentally measured angular distribution, which would help to fix the optical-model parameters more exactly, the parameters we did obtain are consistent with those used in other analyses<sup>10,11</sup> in the same mass and energy region as ours. In particular, the value we used for the nuclear-deformation parameter,  $\beta=+0.30$ , is in agreement with our previous work<sup>6</sup> as well as with

the values obtained by other methods.<sup>5,38,39</sup> We can thus conclude that the adiabatic coupled-channel calculation does indeed explain our experimental data well.

On the other hand, as we have seen in Sec. VB, the experimental value for  $\Delta\sigma_t/\sigma_t$  is about 50% larger than that predicted by the black-nucleus model, indicating that 14 MeV is not yet high enough in energy for the neutrons to satisfy the conditions of applicability of this model (that is,  $kR \gg 1$  and a very strong absorption). Although this result is not unexpected, one can immediately raise the question as to what is the exact energy at which this model does become applicable. From the condition  $kR \gg 1$ , one would expect that the energy would have to be a few tens of MeV. However, as we mentioned in the Introduction, as one goes to higher energies the nucleus may become semitransparent to the neutron. Thus, there might be some doubt whether there exists any neutron energy region at all where the black-nucleus model is applicable.

If elastic-scattering differential-cross-section data were available at higher energies (for example, in 5-MeV steps up to about 100 MeV), then one could perform the coupled-channel calculation to obtain optical-model parameters by fitting the data. The parameters thus fixed could in turn be used in predicting the theoretical behavior of  $\Delta\sigma_t/\sigma_t$  as a function of energy to see if it will ever converge to the black-nucleus value given in (23). However, we should not be able to predict  $\Delta\sigma_t/\sigma_t$  accurately enough to show conclusively that we are in the black-nucleus energy region because the optical-model parameters obtained from the fit of the above elastic-scattering data would not be unique. On the other hand, measurements of  $\Delta\sigma_t/\sigma_t$  and  $\sigma_t$  seem to give a rather clear-cut criterion on this question, as we have discussed in Sec. V. It would thus be quite interesting to extend our present measurements<sup>40</sup> to higher energies. Since higher energy neutron sources are available,<sup>41</sup> such an extension does seem feasible.

The experimental results of Shelley *et al.*,<sup>7</sup> in which they measured  $\sigma_t$  and  $\Delta\sigma_t/\sigma_t$  at 15 MeV, can be compared to our results at 14 MeV. In their work the holmium nuclei were polarized along the beam direction, whereas in ours they were aligned perpendicular to the beam direction. If we ignore the small contribution of the higher order nuclear alignment parameters ( $f_4$  and  $f_6$ ), our measured value of  $\Delta\sigma_t$  normalized to

<sup>38</sup> E. G. Fuller and E. Hayward, Nucl. Phys. **30**, 613 (1962); M. Danos and W. Greiner, Phys. Letters **8**, 113 (1964).

<sup>39</sup> B. Elbek, *Determination of Nuclear Transition Probabilities by Coulomb Excitation* (Ejnar Munksgaards Forlag, Copenhagen, 1963).

<sup>40</sup> It would be rather difficult to use our present holmium crystal for these measurements. If no larger crystal is available we would have to use a polycrystalline sample in a high magnetic field as was done in Ref. 7. The slight disadvantage in using a thick polarized sample was discussed in the Introduction.

<sup>41</sup> For example, using high-current pulsed machines, such as linacs and synchrocyclotrons, and time-of-flight techniques. The use of such neutron sources would allow us to cover a large energy region at one time and also overlap the discrete-energies where previous measurements have been made.

<sup>37</sup> The bars over the  $f$ 's were omitted in Eq. (6a) of Ref. 5 owing to a typographical error.

complete nuclear alignment (the  $m = \pm 7/2$  substates are the only ones populated in this case) perpendicular to the beam is  $\Delta\sigma_i = +(343 \pm 73)$  mb. For the case of complete alignment parallel to the beam,  $\Delta\sigma_i$  would be decreased by twice this amount; that is,  $\Delta\sigma_i = -(686 \pm 146)$  mb. Their result when normalized to complete nuclear alignment parallel to the beam is  $\Delta\sigma_i = -(573 \pm 138)$  mb. These two results are in good agreement when one considers the errors involved in the measurements.

#### ACKNOWLEDGMENTS

We should like to acknowledge the help of Dr. R. B. Schwartz and E. Ritter during the early stages of the experiment. The technical assistance of R. B. Dove, F. P. Karns, A. Wasilewski, and J. K. Whittaker is deeply appreciated. One of us (H.M.) would like to acknowledge helpful discussions with Dr. E. Ambler, Dr. J. C. Eisenstein, and Dr. E. G. Fuller.

#### APPENDIX: THE INSCATTERING CORRECTION

Expressions for the inscattering correction to transmission measurements of total-neutron cross sections have been derived previously.<sup>42</sup> However, there are apparently no reported results for the case of a narrow collimated beam of neutrons with both sample and detector lengths not negligible compared to their separation. We assume that the collimated neutron beam can be approximated by a beam along the axis of the system, that the number of neutrons detected per unit path length in the detector is constant and independent of energy, and that the small correction depending on  $\cos\theta$  in the exponential attenuation by the sample following single scattering is negligible. It can then be readily shown that the correction  $\delta\sigma$  for single inscattering is given by

$$\delta\sigma = -\frac{2\pi}{ls} \int_0^t dx \int_0^s dy \int_0^{\theta'(x,y)} \sigma(\theta) \tan\theta d\theta, \quad (\text{A1})$$

where  $t$  is the scattering sample length,  $s$  the detector length,  $\sigma(\theta)$  the differential scattering cross section for all events above the detector cutoff bias, and  $\theta'(x,y) = \arctan[b/(l-x+y)]$  with  $b$  the (cylindrical) detector radius and  $l$  the distance from the front of the scattering sample to the front of the detector. This result reduces to the usual form for inscattering,

$$\delta\sigma = -\sigma(0)\pi b^2/L^2, \quad (\text{A2})$$

for  $t/l$ ,  $s/l$ , and  $b/l$  small, where  $L$  is now the distance from the center of the sample to the center of the detector. The  $y$  dependence in (A1) can be eliminated and the resulting expression is more amenable to numerical

evaluation<sup>43</sup>:

$$\delta\sigma = -\frac{2\pi}{l} \int_0^t \left\{ \int_0^{\theta_1(x)} \sigma(\theta) \tan\theta d\theta + \frac{b}{s} \int_{\theta_1(x)}^{\theta_2(x)} [1/\tan\theta - 1/\tan\theta_2] \sigma(\theta) \tan\theta d\theta \right\} dx, \quad (\text{A3})$$

where

$$\theta_1(x) = \arctan[b/(l+s-x)],$$

and

$$\theta_2(x) = \arctan[b/(l-x)].$$

For our case,  $\sigma(\theta)$  has not been measured and it was necessary to generate angular distributions using the theoretical method described in Sec. VA (see Fig. 11). The small ( $n,n'$ ) and ( $n,2n$ ) contributions to the forward cross section were estimated from the work of Howerton<sup>44</sup> and experimental data for Ta and Bi.<sup>45</sup> The calculated values for  $\delta\sigma$  using these angular distributions in (A1) were, for the thin and thick sample, respectively, 9% and 12% smaller than those given by inserting  $\sigma(0)$  into the simpler expression (A2). It is estimated that the value of  $\delta\sigma$  obtained using (A1) has an uncertainty of about  $\pm 10\%$ , due mainly to uncertainties in  $\sigma(\theta)$ . Errors due to the approximations used in deriving (A1) lead, at most, to overestimation of  $\delta\sigma$  by a few percent for our beam and detector geometry.

The contribution of the second-order inscattering was estimated by numerically integrating the expression

$$\frac{T_2}{T_1} = \frac{\pi n l}{\sigma(0)} \int_0^{\theta_m} \sigma(\theta)^2 \sin\theta d\theta, \quad (\text{A4})$$

where  $T_1$  and  $T_2$  are the corrections to the measured transmission due to first- and second-order inscattering,  $n$  is the density of scattering nuclei, and  $\theta_m$  is the first diffraction minimum in  $\sigma(\theta)$ .<sup>42</sup> This correction amounted to 0.3% and 0.8% for our thin and thick polycrystalline samples, respectively. Contributions from higher order inscattering are, by comparison, negligible.

The correction to  $\Delta\sigma_i/\sigma_i$  for inscattering was evaluated using (A3) to correct the transmissions in the appropriate form of (5). The small correction for inscattering by the copper plates holding the holmium single metal crystal was evaluated using (A2). Most of the change in  $\sigma(\theta)$  near zero degrees due to nuclear alignment is directly proportional to the corresponding change in total cross section. It can easily be shown that the ratio  $\Delta\sigma_i/\sigma_i$  is independent of such changes, and only depends on changes in the shape of the angular distribution. For this reason the inscattering correction to  $\Delta\sigma_i/\sigma_i$  is small; for our case it amounted to about 7%.

<sup>43</sup> This expression was evaluated using an OMNITAB program on the NBS 7094 computer.

<sup>44</sup> R. J. Howerton, University of California Radiation Laboratory Report No. UCRL-5351, 1958 (unpublished).

<sup>45</sup> L. Rosen and L. Stewart, Phys. Rev. **107**, 824 (1957).

<sup>42</sup> A convenient summary is given by D. W. Miller, in *Fast Neutron Physics* edited by J. B. Marion and J. L. Fowler (Interscience Publishers, Inc., New York, 1963), p. 997.